IEEE Photonics Journal
An IEEE Photonics Society Publication

Open Access

SSB Pruned DFT-Spread FBMC Signal With Low PAPR in Direct-Detection PONs

Volume 12, Number 3, June 2020

Xiaoling Zhang
Chongfu Zhang, *Senior Member, IEEE*
Mingyue Zhu
Wei Jin
Chen Chen
Xiang Gao
Kun Qiu

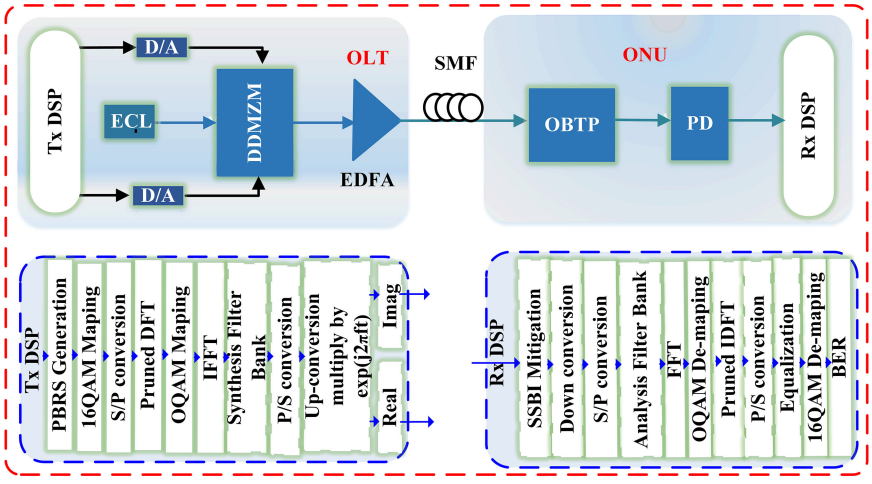

DOI: 10.1109/JPHOT.2020.2993075

SSB Pruned DFT-Spread FBMC Signal With Low PAPR in Direct-Detection PONs

Xiaoling Zhang,[1] Chongfu Zhang ,[1,2] *Senior Member, IEEE*, Mingyue Zhu,[1] Wei Jin ,[3] Chen Chen ,[4] Xiang Gao ,[1] and Kun Qiu[1]

[1]School of Information and Communication Engineering, Zhongshan Institute, University of Electronic Science and Technology of China, Chengdu 611731, China
[2]School of Electronic Information, Zhongshan Institute, University of Electronic Science and Technology of China, Zhongshan 528402, China
[3]School of Electronic Engineering, Bangor University, LL57 1UT, Bangor, UK
[4]School of Microelectronics and Communication Engineering, Chongqing University, Chongqing 400030, China

DOI:10.1109/JPHOT.2020.2993075

Manuscript received March 30, 2020; accepted May 3, 2020. Date of publication May 7, 2020; date of current version May 26, 2020. This work was supported in part by the National Key R&D Program of China under Grant 2018YFB1801302, in part by Project for Innovation Team of Guangdong University (2018KCXTD033), in part by Project for Zhongshan Social Public Welfare Science and Technology (2019B2007), in part by Zhongshan Innovative Research Team Program (180809162197886), and in part by Research Project for Talent of UESTC Zhongshan Institute (418YKQN07). Corresponding author: Chongfu Zhang (e-mail: cfzhang@uestc.edu.cn).

Abstract: Filter bank multi-carrier (FBMC) using offset quadrature amplitude modulation (OQAM) has recently attracted increasing interests for the next-generation high-speed optical transmission systems, due to the salient FBMC modulation advantages in terms of high spectrum efficiency by completely removing the cyclic prefix. However, high peak-to-average power ratio (PAPR) still plays a key role of constraining the performance of FBMC systems. In this paper, we investigate a single sideband (SSB) pruned discrete Fourier transform (DFT)-spread FBMC for direct-detection (DD) passive optical network systems (PONs). It is demonstrated that the PAPR of the SSB pruned DFT-spread FBMC signal with the overlapping factor of 1.56 outperforms the conventional FBMC signal and the simple DFT-spread FBMC signal by $\sim$2 dB and 1 dB at the complementary cumulative distribution function (CCDF) of 1×10^{-3}, respectively. Finally, by using the pruned DFT-spread FBMC with low PAPR, the aggregate data rate of 50-Gbit/s can be achieved after 50-km single mode fiber (SMF) transmission below the 7% hard decision forward-error correction (HD-FEC) threshold in the DD PONs.

Index Terms: FBMC, PAPR, direct detection, passive optical network.

1. Introduction

Driven by the emerging bandwidth-hungry applications such as high-definition video (HDV), cloud computing and 5G mobile fronthaul (MFH) networks, many researchers are expecting to increase the overall network capacity and enhance the transmission performance of the next generation access network [1]–[4] in a cost-effective manner. Passive optical networks (PONs), as the last-mile access network, are facing many opportunities and challenges. As such, it is expected that the next generation PONs can not only have a capability of offering high speed and reliability, but

also provide excellent compatibility for all-existing PON systems with different signal transmission speeds and various modulation/detection techniques [5], [6]. In order to achieve this goal, many major standardization bodies are actively upgrading the roadmap of the next generation access network. Recently, the body of IEEE has carried out efforts beyond the 10 Gbit/s PON, by making the IEEE P802.3ca standardization effort of 25, 50, and 100G EPON with expectations to be fully released by the end of April of 2020 [7]. Another body of the ITU-T is also considering the roadmap smooth evolution of the 10G NG-PON2 to high-speed and long-reach optical access network, with proposals of taking coherent optical communication technologies as a promising solution to satisfy the ever-increasing demands of the next generation optical access network [8]. However, the inherent high complexity and network overall costs of the coherent optical communication systems are still the main challenges for the implementation in cost-sensitive PON application scenarios [9]. On the one hand, single sideband (SSB) modulation and direct-detection (DD) optical communication systems with low cost and low network complexity are still attracted plenty of researchers' interests in the field of short-haul optical access networks. On the other hand, lots of researchers have paid extensive efforts to propose and upgrade many advanced modulation techniques for achieving higher spectral-efficiency (SE) in optical transmission systems, such as quadrature amplitude modulation (QAM) subcarrier modulation [10]–[14], carrier-less amplitude and phase (CAP) modulation [15]–[18], orthogonal frequency division multiplexing (OFDM) [18]–[20] and filter bank multicarrier (FBMC) modulation [21]–[23]. Among those modulation techniques, multicarrier OFDM and FBMC have gained the favor due to their salient features in terms of high SE, excellent network flexibility and adaptability as well as strong system robustness to the transmission impairments such as chromatic dispersion (CD). Weng *et al*. have experimentally demonstrated a 60-Gbit/s dispersion-managed long-reach OFDM-PON with an injection-locked quasi-color-free laser diode (QCFLD) [24]. Lin *et al*. have recently studied a 27.15-Gbits/s spread-OFDM in PON transmission systems with sub-Nyquist receiver based on digital pre-processing over 10-km standard single mode fiber (SSMF) [19]. Jung *et al*. have used an adaptively modulated optical FBMC based multiple access (AMO-FBMC-MA) in PON uplink transmission to reduce multiple access interference [25. Extensive performance comparisons have also been made by Saljoghei *et al*. between FBMC and OFDM in multiple access uplink PONs [23], and the results show that FBMC is a more promising signal format due to its unique features of loosening requirements on synchronization, suppression of out-of-band interference and free from cyclic prefix. However, an inherent defect of the multi-carrier multiplexing modulation techniques is their high peak-to-average power ratio (PAPR). High PAPR delivers a great disadvantage for optical transmission systems because it raises the requirements on the electrical/optical devices with large dynamic operation ranges, such as digital-analog converters/analog-digital converters (DACs)/(ADCs), Mach–Zehnder modulator (MZM) and optical/electrical amplifiers.

In addition, high PAPR also leads the transmission system to be more susceptible to nonlinear impairments and therefore considerably degrades the transmission performance. A large diversity of PAPR reduction methods have been proposed, such as clipping [26], selective mapping (SLM) [27]–[29], companding transformation coding [30] and discrete Fourier transform (DFT) spreading [31]–[34]. Especially, for the most promise candidate waveform for the next-generation network, researchers are extensive investigating new types of FBMC with low PAPR [35]–[37].

In this paper, we investigate the pruned DFT spreading technique for low-PAPR FBMC based DD PON systems. Due to the employment of pruned discrete Fourier transform spread FBMC (pruned DFT-spread FBMC) signal, the system has the advantages of (1) low PAPR without any side information and (2) low out-of-band (OOB) emissions which are comparable to SC-FDMA. A 50-Gbit/s optical pruned DFT-spread FBMC signal coded by 16-ary quadrature amplitude modulation (16-QAM) is successfully transmitted over 50-km single mode fiber (SMF) with its BER performance below hard-decision forward-error correction (HD-FEC) threshold of BER $= 3.8 \times 10^{-3}$. And the PAPR of the pruned DFT-spread FBMC signal outperforms the conventional FBMC signal and the simple DFT-spread FBMC signal. The structure of this paper is organized as follows. In section II, we briefly describe the operation principle of the pruned DFT-spread FBMC technique

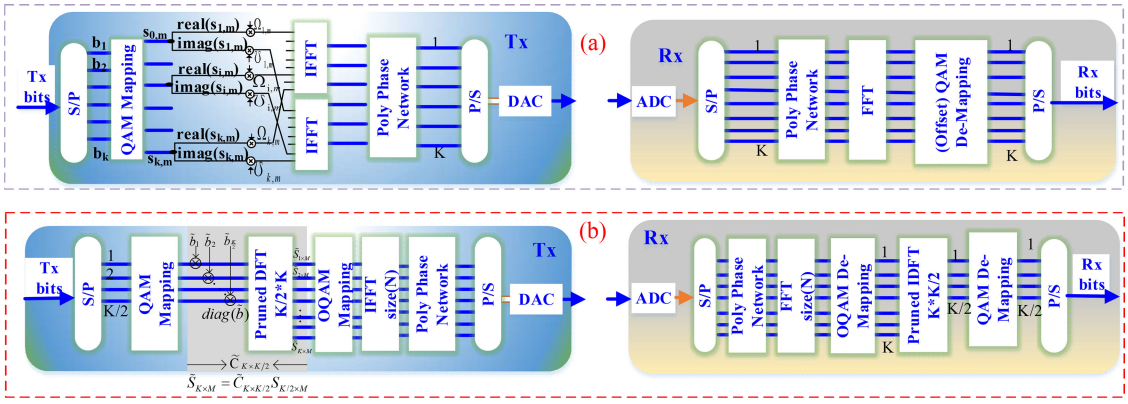

Fig. 1. The transmitter and receiver DSP signal processing procedures. (a) FBMC. (b) Pruned discrete Fourier transform spread FBMC.

for the DD PON systems. Section III shows the simulation setup and Section IV provides the simulation results. Conclusion of this paper is given in Section V.

2. Operation Principle

2.1 Transmitter for FBMC

Fig. 1(a) shows the schematic diagram of the transceiver DSP procedures for the conventional FBMC system, where the input binary random bits are first converted into K parallel bit streams (b_0, b_1, …, b_K) for the K subcarriers and subsequently the bits for each subcarrier are coded to QAM or pulse amplitude modulation (PAM) symbols. To generate the FBMC signal, the real and imaginary parts of the complex QAM symbols or two adjacent PAM symbols of the k-th subcarrier are staggered and respectively multiplied by the matrices $\Omega_{k,m}$ and $\mho_{k,m}$, so as to obtain the OQAM symbol.$\Omega_{k,m}$ and $\mho_{k,m}$ are expressed as

$$\begin{aligned}\Omega_{k,m} &= (-1)^m j^k \text{ or } j^{k+2m}\\ \mho_{k,m} &= (-1)^m j^{k+1} \text{ or } j^{k+2m+1}\end{aligned} \tag{1}$$

Prior to the poly-phase network (PPN) for the synthesis filter bank (SFB) [38], a typical inverse fast Fourier transform (IFFT) process is implemented. At last, the generated time-domain FBMC signal s(t) is expressed as

$$\begin{aligned}s(t) = &\sum_{k=0}^{K-1}\left\{\sum_{m=0}^{M-1}\Omega_{k,m} real(s_{k,m})\hbar(t-mT_0)\right\}e^{jk\frac{2\pi}{T_0}t}\\ &+\sum_{k=0}^{K-1}\left\{\sum_{m=0}^{M-1}\mho_{k,m} imag(s_{k,m})\hbar(t-mT_0-\frac{T_0}{2})\right\}e^{jk\frac{2\pi}{T_0}(t-\frac{T_0}{2})}\end{aligned} \tag{2}$$

Where $\hbar$ is the PPN and T_0 corresponds to the symbol duration of each FBMC signal.

The signal processing procedures of the pruned DFT-spread FBMC system are depicted in Fig. 1(b). First, all the bit sequences are modulated at the half of K subcarriers for QAM mapping. To spread the symbols on the K/2 subcarriers to K subcarriers, a pruned DFT coding matrix $C_{K\times K/2}$ is utilized, which is different from the conventional DFT-matrix, where K/2 columns are canceled. Assuming that the symbols after the QAM mapping is matrix $S_{K/2\times M}$, and the pruned DFT coding

matrix $\widetilde{C}_{K\times K/2}$ can be express as

$$S_{K/2\times M}=\begin{bmatrix} s_{1,1} & s_{1,2} & \cdots & s_{1,M} \\ \vdots & \vdots & \ddots & \vdots \\ s_{i,1} & s_{i,2} & \cdots & s_{i,M} \\ \vdots & \vdots & \ddots & \vdots \\ s_{K/2,1} & s_{K/2,2} & \cdots & s_{/2,M} \end{bmatrix} \tag{3}$$

$$\tilde{C}_{K\times K/2}=\begin{bmatrix} c_{1,1} & c_{1,2} & \cdots & c_{1,K/2} \\ \vdots & \vdots & \ddots & \vdots \\ c_{i,1} & c_{i,2} & \cdots & c_{i,K/2} \\ \vdots & \vdots & \ddots & \vdots \\ c_{K,1} & c_{K,2} & \cdots & c_{K,K/2} \end{bmatrix} \tag{4}$$

Therefore, the symbols after the pruned DFT coding matrix can be written as

$$\tilde{S}_{K\times M}=\tilde{C}_{K\times K/2}S_{K/2\times M} \tag{5}$$

The relationship between the pruned DFT coding matrix $\tilde{C}_{K\times K/2}$ and a full spreading and de-spreading DFT matrix $C_{K\times K}$ can be expressed as,

$$\widetilde{C}_{K\times K/2}=C_{K\times K}\begin{bmatrix} I_{K/2} \\ O_{K/2} \end{bmatrix} diag\left\{\widetilde{b}\right\} \tag{6}$$

where $I_{K/2}$ is an identity matrix, $O_{K/2}$ is an all-zero matrix and $\widetilde{b}$ is the one-tap scaling factor. After pruned DFT coding, the pruned DFT-spread signals are converted into the time domain by an IFFT operation. The output of the IFFT block is then fed into the well-designed SFB. Here a truncated Hermite prototype filter [35] is applied for digital filtering process for each subcarrier. The Hermite prototype filter is expressed as

$$\hbar\left(t\right)=\frac{1}{\sqrt{T_0}}e^{-2\pi\left(\frac{t}{T_0}\right)^2}\sum_{\substack{i=\{0,4,8,\\12,16,20\}}}a_iH_i\left(2\sqrt{\pi}\,\frac{t}{T_0}\right) \tag{7}$$

where the coefficients are

$$\begin{aligned} a_0&=1.412692577 & a_{12}&=-2.2611\cdot10^{-9} \\ a_4&=-3.0145\cdot10^{-3} & a_{16}&=-4.4570\cdot10^{-15} \\ a_8&=-8.8041\cdot10^{-6} & a_{20}&=1.8633\cdot10^{-16} \end{aligned}$$

and the adopted truncated Hermite prototype filter $h_{Trunc.}(t)$ is given by

$$h_{Trunc.}(t)=\begin{cases} h(t) & \text{if } -\Theta T_0\le t\le\Theta T_0 \\ 0 & \text{otherwise} \end{cases} \tag{8}$$

where Θ is the overlapping factor, which should not be larger than 1.56 so as to avert the interference due to IFFT repetition in FBMC [35]. After digital filtering, parallel-to-serial (P/S) conversion is performed before digital-to-analog conversion (DAC).

What's more, the SSB modulation is a promising technique for improving the optical transmission system performance. And a simple and effective structure of the dual-drive Mach-Zehnder modulator (DDMZM) has been used to generate optical SSB signal [39]. As shown in Fig. 2, the optical

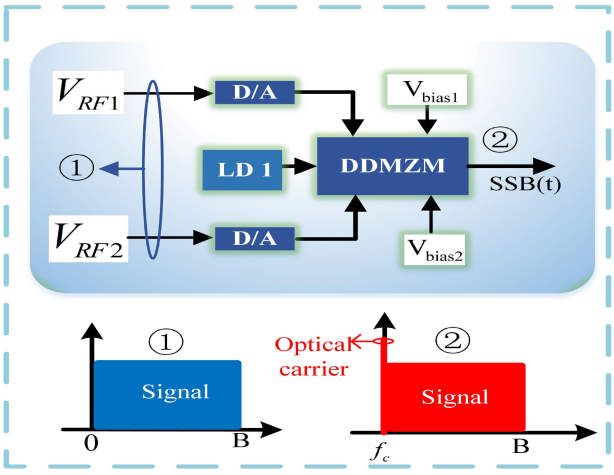

Fig. 2. Schematic diagram of the generation of optical SSB signal using a DDMZM with up-conversion.

SSB signal at the output of the DDMZM can be expressed as

$$S_{out}(t) \approx \frac{E_{in}(t)}{2}\left[-j\left(1+\frac{j\pi}{V_\pi}V_{RF1}\right)+1+\frac{j\pi}{V_\pi}V_{RF2}\right]$$
$$= \frac{E_{in}(t)}{2}\left[1-j+\frac{\pi}{V_\pi}\left(V_{RF1}+jV_{RF2}\right)\right] \quad (9)$$

where $E_{in}(t)$ is the optical carrier, V_π is the half-wave voltage of DDMZM, V_{RF1} and V_{RF2} are the real and imaginary parts of the up-converted pruned DFT-spread FBMC signal, respectively. At the receiver end, a single photodetector (PD) is used to convert the obtained optical SSB signal into electrical signal. After analog-digital conversion (ADC), the received signal is processed in the DSP. Kramers–Kronig (KK) receiver is utilized to mitigate the signal-signal beat interferences (SSBI) component [39], followed by a baseband down-conversion operation. The following digital signal processing contains serial-to-parallel (S/P) conversion and analysis filter bank (AFB) filtering. In conventional FBMC systems, after the Fast Fourier transform (FFT) block, the OQAM demodulation and P/S conversion are carried out for analyzing the BER performance. While in the pruned DFT-spread FBMC systems, after the FFT process, the pruned IDFT should be implemented before the QAM demodulation. Assuming $R_{K\times M}$ is the data sequence after the FFT operation, the signal after performing pruned IDFT decoding can be express as

$$\widetilde{R}_{K/2\times M} = \tilde{C}^H_{K\times K/2} R_{K\times M} \quad (10)$$

where the matrix $\tilde{C}^H_{K\times K/2}$ is the conjugate transpose of the coding matrix $\tilde{C}_{K\times K/2}$.

2.2 PAPR

In general, the PAPR in multi-carrier modulation technology is defined as

$$PAPR(dB) = 10\log_{10}\left[\frac{\max_{0\le n\le N-1}|s_n|^2}{E\left(|s_n|^2\right)}\right] \quad (11)$$

which is an essential factor to evaluate the performance of a multi-carrier modulation system. In (11), S_n is the FBMC signal with N subcarriers and $E(|s_n|^2)$ denotes the average power of the signal. Usually, we are interested in the complementary cumulative distribution function (CCDF), which is the probability of the PAPR of signal frames exceeding a specific threshold $PAPR_0$:

$$CCDF = \Pr[PAPR > PAPR_0] \quad (12)$$

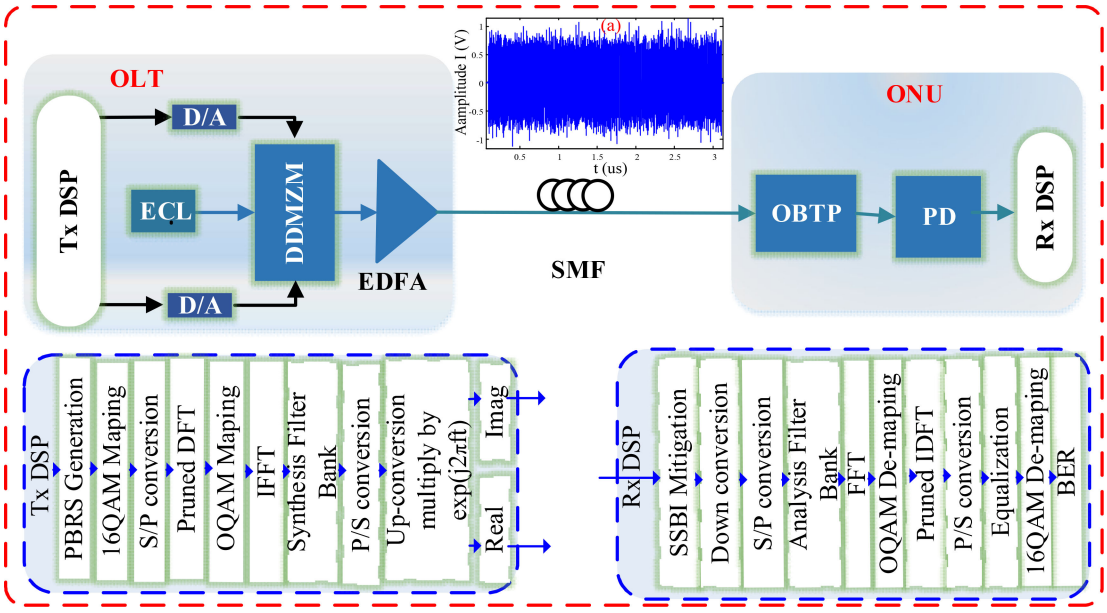

Fig. 3. Schematic diagram of the pruned DFT-spread FBMC for single-sideband direct-detection PON system. (a) Waveform of the real part of the pruned DFT-spread FBMC.

TABLE 1
Transceiver and Optical Device Parameters

Parameter	Value
DAC/ ADC sampling rate	40 GSa/s
DAC/ ADC bit resolution	8 bits
IFFT/FFT points	512
ECL laser operation wavelength	1552.524 nm
Chromatic dispersion	17 ps/nm/km
SMF attenuation	0.2 dB/km
Dispersion slope	0.08 ps/nm^2/km
Kerr coefficient	2.6 × 10^{-20} m^2/W
Effective core area	80.0 μm^2
Noise figure of EDFA	4 dB
OBPF type	Gaussian
OBPF bandwidth	20 GHz
PIN detector responsivity	0.8 A/W
PIN detector sensitivity	-19 dBm

The performance of the PAPR in the pruned DFT-spread FBMC system is studied in Section IV.

3. Simulation Verification

Fig. 3 shows the proof-of-concept simulation setup of the SSB pruned DFT-spread FBMC in DD PON transmission systems. The simulation is implemented via the commercial simulation software VPI Transmission Maker version 9.0 and MATLAB. The main system parameters are summarized and listed in Table 1. At the optical line terminal (OLT), the SSB pruned DFT-spread FBMC signals for the optical network units (ONUs) are generated, where the input pseudo random binary sequence (PRBS) stream is firstly coded by 16-QAM. After S/P conversion, QAM mapping is performed. Thereafter, the pruned DFT-spread coding matrix is utilized before the IFFT to generate the pruned DFT-spread FBMC signal. After that, 64 subcarriers with effective data are spread into 128 subcarriers. And the IFFT operation with the size of 512 is employed to produce the

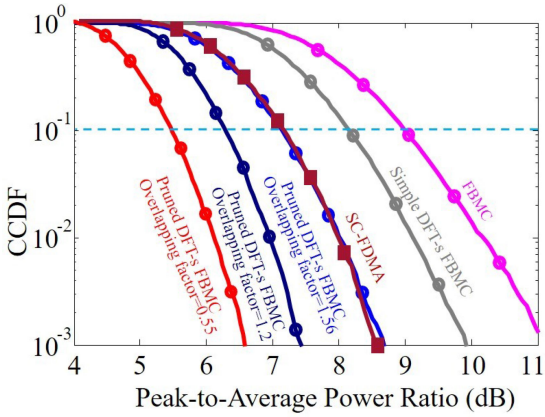

Fig. 4. The performance of PAPR with three FBMC signals.

time-domain signal. Then each subcarrier of the signal is digitally filtered by a SFB based on the truncated Hermite prototype filter. Subsequently, the generated pruned DFT-spread FBMC signal is up-converted by multiplexing $\exp(j2\pi ft)$ after P/S conversion. The real and imaginary parts of the generated digital signals are fed into the DACs, which are operating at 40 GSa/s@ 8 bit. The adopted DDMZM is biased at its quadrature bias point for SSB signal generation and its half-wave voltage is 5.0 V. The central wavelength of the light source is 1552.524 nm with a linewidth of 100 kHz, and the launch optical power of the light source is 12 dBm. The generated optical SSB pruned DFT-spread FBMC signals are amplified by an erbium-doped fiber amplifier (EDFA). Then the optical SSB pruned DFT-spread FBMC signal is delivered into the SMF. The SMF has an attenuation coefficient of 0.2 dB/km, a dispersion of $16e^{-6}$ s/m^2, a dispersion slope of 0.08 ps/nm^2/km, a Kerr coefficient of $2.6e^{-20}$ m^2/W and an effective core area of 80.0 um^2. In the ONU side, a Gaussian shape optical band-pass filter (OBPF) with 20-GHz bandwidth is used to remove the out-of-band noise. Then the obtained optical SSB pruned DFT-spread FBMC signal is detected by a PIN with a bandwidth of 20 GHz and a responsivity of 0.8 A/W. ADCs with 40 GSa/s sampling rate and 8-bit resolution are utilized for digitization. After that, the received electrical signal is further processed in the receiver DSP. First, KK-algorithm is utilized to mitigate the effect of SSBI, where each received symbol has four digital samples to satisfy the requirements of the KK algorithm. Then down conversion and S/P conversion are performed, which are followed by AFB, FFT and pruned IDFT operations. Finally, BER performances of the pruned DFT-spread FBMC signals are explored after P/S conversion, signal equalization and 16-QAM decoding.

4. Results and Discussion

Fig. 4 shows the PAPR performances for different FBMC signals each containing 128 16-QAM-coded subcarriers and obtained by performing 512-point IFFT operation. As we can see, for a specific CCDF of 1×10^{-1}, the PAPR of the conventional FBMC (non-pruned DFT-spread FBMC) is about 9.2 dB. While for the pruned DFT-spread FBMC signal with the overlapping factor of 1.56, 1.2 and 0.55, the PAPR improvements are $\sim$2 dB, $\sim$2.8 dB and $\sim$3.6 dB, respectively. It is also very interesting to find that the PAPR performance of the pruned DFT-spread FBMC outperforms the simple DFT-spread FBMC [40] techniques, even for the single-carrier frequency division multiple access (SC-FDMA) techniques, which generates DFT-S conventional OFDM signals. For fair comparison, the SC-FDMA signal subcarriers and the adopted IFFT point size are equal to the FBMC signals.

To evaluate the impact of the overlapping factor of the truncated Hermite prototype filter on the SSB pruned DFT-spread FBMC signal transmission performance in the DD PON system, we first

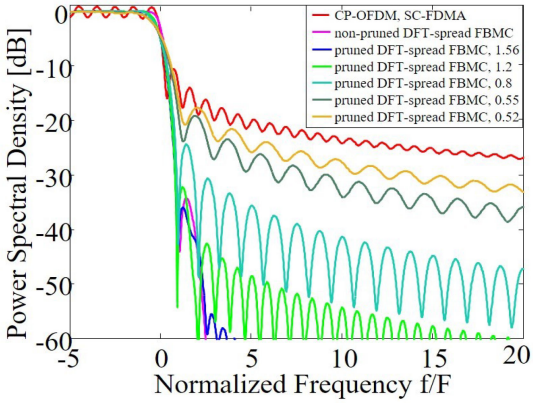

Fig. 5. PSD of the Hermite filter with different overlapping factor.

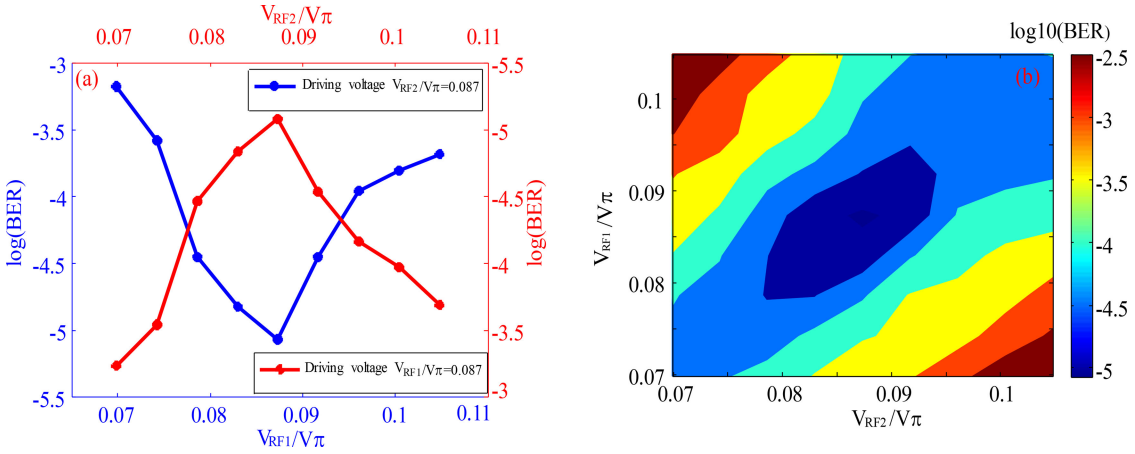

Fig. 6. (a) BER as a function of driving voltage. (b) BER vs. the driving voltage V_{RF1}/V_π and V_{RF2}/V_π.

explore the power spectral density (PSD) of the Hermite prototype filter with different overlapping factors. As shown in Fig. 5, the PSD of the truncated Hermite prototype filter with the overlapping factors of 1.56 and 1.2 has minor difference between the first-order side lobes, and even with an overlapping factor of 0.8, the power leakage of pruned DFT spread FBMC is still relatively low. When the overlapping factor of 0.55 is used, the normalized power of the first order side lobe is approximate -22 dB. While for the overlapping factor of 0.52, the normalized power of first-order side lobe is increased to -20 dB, and compared to the OFDM, the pruned DFT spread FBMC still has better power leakage of emissions. From Figs. 4 and 5, it can be observed that a large overlapping factor leads to a considerable reduction in digital filter side lobes, but it simultaneously degrades the PAPR performances. Therefore, it is necessary to properly select the overlapping factor for optimum trade-off between power leakage of digital filter emissions characteristics and PAPR performance, which will have a vital impact on the performance of the system.

In the SSB pruned DFT-spread FBMC based DD PON systems with DDMZM, the driving voltage of two arms of the DDMZM should be investigated. Fig. 6 shows the BER as a function of the driving voltage of pruned DFT-spread FBMC signal, we can see that in Fig. 6(a) when the driving voltage V_{RF1}/V_π and V_{RF2}/V_π all are about to 0.087 the performance are optimal. Increasing/decreasing driving voltage of signal induces the performance deteriorate. To further investigate the BER performance as a function of the signal driving voltage, the results are illustrated in Fig. 6(b), which

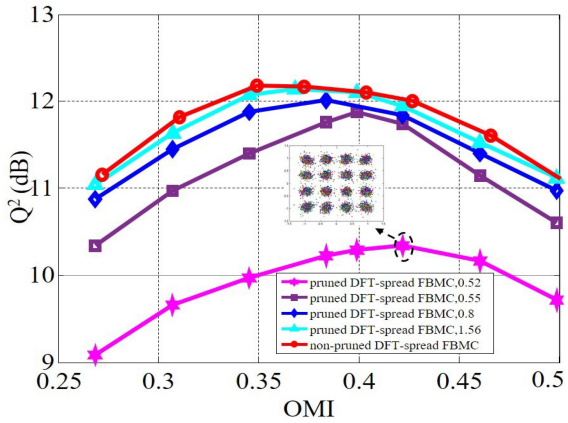

Fig. 7. BER versus OMI in back-to-back systems. The optical launch power and received optical power is fixed at 0 and −14 dBm, respectively.

show that the driving voltage of signal V_{RF1}/V_π equal to V_{RF2}/V_π the system with the preferable performance, V_{RF1}/V_π and V_{RF2}/V_π imbalance induce the performance deteriorate. Therefore, it necessary to ensure the driving voltage of the two arms of the DDMZM are equal.

Since the optical modulation index (OMI) plays a main factor in determining the performances in DD PONs, which reflects the linearity operation regime of the DDMZM and affects the carrier to signal power ratio (CSPR) of the optical SSB signal. We then investigate the influence of the OMI on the Q^2-factor performance of the SSB pruned DFT-spread FBMC signals in optical back-to-back (OB2B) systems to make sure that the system operates at the best conditions and also satisfies the requirement of the KK operation, the results are illustrated in Fig. 7. The Q^2-factor is defined as a function of BER i.e.,$Q^2 = 20\log_{10}[\sqrt{2}erfc^{-1}(2BER)]$, while the OMI is defined as $OMI = \pi V_{RF}^{rms}/V_\pi$, where V_{RF}^{rms} is the root-mean-square (RMS) of the electrical signals input to the DDMZM. The optical launch power and received optical power for the SSB pruned DFT-spread FBMC signals are fixed at 0 dBm and −14 dBm, respectively. Meanwhile, the performance of the truncated Hermite filtering with different overlapping factors are also explored. We can find that for the SSB pruned DFT-spread FBMC signals with different overlapping factors, there exist different optimal OMI to achieve the maximum Q^2-factor, which is approximately 0.36, 0.38, 0.40 and 0.42 for overlapping factor of 1.56, 0.8, 0.55 and 0.52, respectively. Meanwhile, the non-pruned DFT-spread FBMC is also simulated for reference, the optimal OMI is slightly smaller than that of pruned DFT-spread FBMC with the overlapping of 1.56. Below the optimum OMI, the system performance is limited by signal-to-noise ratio of the modulated signal, while for the large OMI, the system suffers from modulator nonlinearity. In the following, the OMI is optimized at different transmission cases.

Fig. 8 shows the BER performances versus different laser linewidth and fiber length for the SSB pruned DFT-spread FBMC with the overlapping factor of 1.56. The phase noise introduced by the ECL combined with fiber CD can degrade the system performance. In general, ECL phase noise can be modeled by a Wiener process with zero mean and variance of $t\Delta\nu/(2\pi)$, where t and $\Delta\nu$ denotes the time and laser linewidth, which joint the effect of the fiber chromatic dispersion. After the square-law detection in the DD PON system, it will induce phase-to-amplitude noise. As we can see, for the linewidth enlarging from 0.1 to 0.5 MHz and fiber length from 10 to 25 km, the corlor map is from green region to cyan region, which means the $\log_{10}$(BER) is enlarging to −4. And for the linewidth enlarging from 2 to 3 MHz and fiber length from 25 to 30 km, the red-color region of the color map, the $\log_{10}$(BER) is larger than −3.6, which implies too large laser linewidth should not be used to achieve high performance and large system reach. In the following, the ECL with linewidth of 100 kHz is utilized.

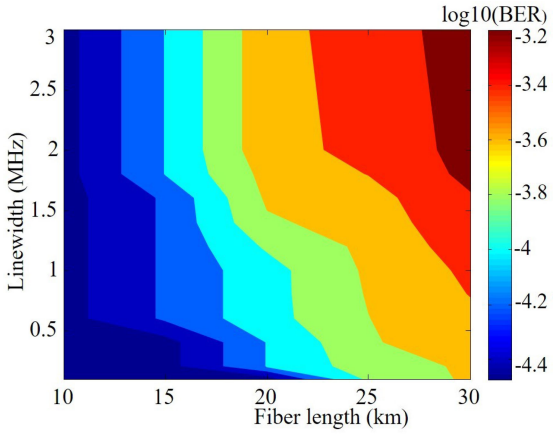

Fig. 8. BER as a function of different laser linewidth and fiber length for the pruned DFT-spread FBMC with overlapping factor of 1.56.

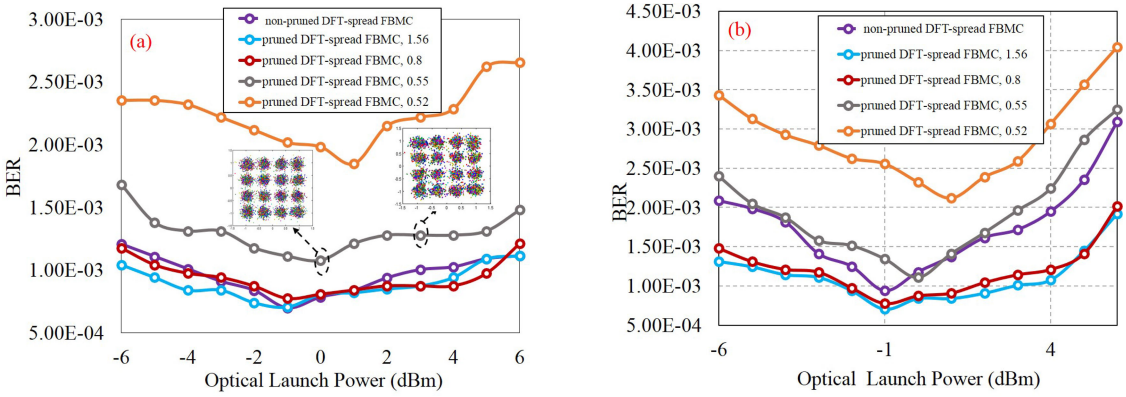

Fig. 9. BER performances as a function of the total launch power for (a) 25-km and (b) 50-km SMF transmissions.

The optimum fiber launch power of the SSB pruned DFT spread FBMC signal in the DD PON system is then identified. A comparison of non-pruned DFT-spread FBMC is also conducted as reference. Fig. 9 presents the BER performance as a function of the optical launch power over 25-km and 50-km SMF transmissions. The received optical powers for the 25-km and 50-km optical fiber link are fixed at −14 and −12 dBm, respectively. As shown in Fig. 9, after the 25-km and 50-km optical fiber links, the optimum launch powers are independent of the digital filter overlapping factors. For the pruned DFT-spread FBMC with the overlapping factor of 0.8 and 1.56, they have the same optimum launch power with the non-pruned DFT- spread FBMC, which is approximate at −1 dBm. While for the pruned DFT-spread FBMC with the overlapping factor of 0.55 and 0.52, the optimum launch power are about 0 and 1 dBm. The corresponding constellation diagram for the overlapping factor of 0.55 at the optical launch power of 0 dBm is also depicted. Note that, when the optical launch power below the optimum value, the system transmission performance is degraded mainly because of the decreased OSNR. When optical launch power beyond the optimum value, the performance degradation is mainly due to the fiber nonlinearity effect [41]. For different overlapping factors, the trends of BERs are similar with the increase of the optical launch power.

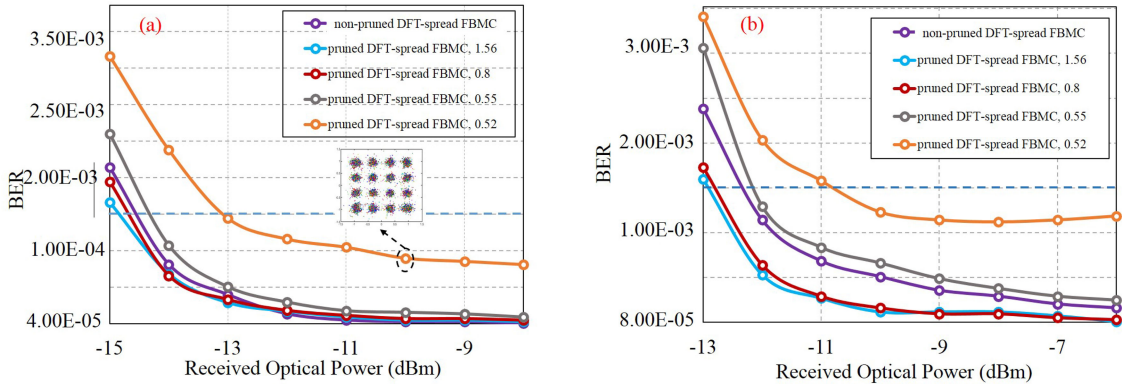

Fig. 10. BER performances as function of received optical power for (a) 25-km fiber link and (b) 50-km fiber link.

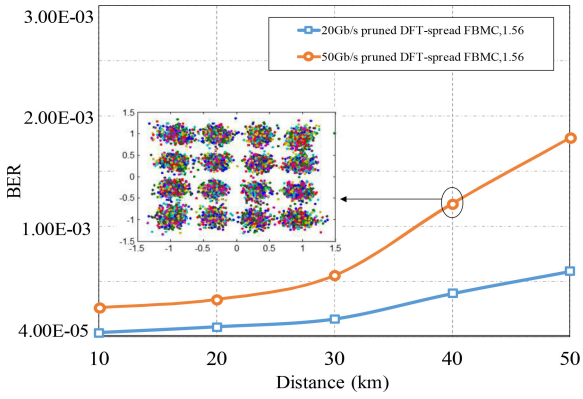

Fig. 11. BER performances as of function of transmission distance.

To further evaluate the performance of the SSB pruned DFT-spread FBMC signals in the DD PON system, the BER performance versus the received optical power after 25-km and 50-km transmission are also investigated and the results are depicted in Fig. 10. It can be observed that the receiver sensitivities at the hard-decision forward-error correction (HD-FEC) threshold of BER $= 1.5 \times 10^{-3}$ is about -13.0, -14.5 and -14.6 dBm for the truncated Hermite filter with the overlapping factor of 0.52, 0.55 and 0.8 after 25-km SMF transmission, respectively. Such receiver sensitivity differences are mainly attributed to the different digital filtering performances of the adopted truncated Hermite filters with various overlapping factors. The BER performances for the overlapping factor of 0.8 and 1.56 are very similar, since the digital filtering-induced power leakage for these two overlapping factors are negligible, as seen in Fig. 5. The constellation diagram of the pruned DFT-spread FBMC signals with overlapping factor of 0.52 at the received optical power of -10 dBm is also depicted. And after 50-km SMF transmission, the receiver sensitivities for overlapping factors of 0.52, 0.55 and 0.8 are about -11, -12.2 and -12.8 dBm, as seen in Fig. 10(b). It can be found that the BER performances for the pruned DFT-spread FBMC with the overlapping factors of 0.8 and 1.56 are better than the non-pruned DFT-spread FBMC after 50-km transmission. It reveals that by using the low-PAPR based pruned DFT-spread FBMC with appropriate overlapping factors, such as 1.56 and 0.8, both the transmission performance and PAPR performance can be enhanced simultaneously.

The results of above are based on 20 Gbit/s. Single-wavelength with 50 Gbit/s is currently considered as an excellent candidate for high speed next-generation PONs. So the performance

of the SSB pruned DFT-spread FBMC signals with 50 Gbit/s should also be considered. Therefore, we investigate the BER performance as the function of transmission distance with data rates of 20 Gbit/s and 50 Gbit/s, as shown in Fig. 11. Where the received optical power is maintained at −10 dBm. It can be seen that the BER of 20 Gbit/s and 50 Gbit/s signal after 50-km transmission below the 7% FEC can be achieved, which provided a promise of supporting 50G-PON downstream transmission for next-generation optical access networks.

5. Conclusions

In this paper, we have investigated the SSB pruned DFT-spread FBMC signal with low PAPR in DD-PONs. The results have shown that the PAPR of the pruned DFT-spread FBMC signal outperforms both the simple DFT-spread FBMC signals and conventional-FBMC signals. The SSB pruned DFT-spread FBMC signal even with the overlapping factor of 0.52 can be successfully transmitted over 25-km and 50-km optical links. The received optical power of as low as −13 dBm and −11 dBm can still achieve the BER performance of 1.5×10^{-3}. Our results show that low-PAPR based pruned DFT-spread FBMC with appropriate overlapping factors can enhance both the PAPR performance and the transmission performance. Therefore, the SSB pruned DFT-spread FBMC scheme with low PAPR is a promising candidate for future cost-effective optical access networks.

References

[1] M. Presi *et al.*, "Field-trial of a high-budget, filterless, λ-to-the-user, UDWDM-PON enabled by an innovative class of low-cost coherent transceivers," *J. Lightw. Technol.*, vol. 35, no. 23, pp. 5250–5259, Dec. 2017.

[2] J. Zhang *et al.*, "200-Gb/s/λ PDM-PAM-4 PON with 29-dB power budget based on heterodyne coherent detection," in *Proc. Opt. Fiber Commun. Conf.*, San Diego, California, 2019, Paper Th3F.1.

[3] Md. G. Saber *et al.*, "Demonstration of a 120° hybrid based simplified coherent receiver on SOI for high speed PON applications," *Opt. Express*, vol. 26, no. 24, pp. 31222–31232, Nov. 2018.

[4] F. Bao *et al.*, "300 Gb/s IM/DD based SDM-WDM-PON with laserless ONUs," *Opt. Express*, vol. 26, no. 7, 2018, Art. no. 7949.

[5] M. Ruffini, "Multidimensional convergence in future 5G networks," *J. Lightw. Technol.*, vol. 35, no. 3, pp. 535–549, Feb. 2017.

[6] V. Houtsma, D. Veen, and E. Harstead, "Recent progress on standardization of next-generation 25, 50, and 100G EPON," *J. Lightw. Technol.*, vol. 35, no. 6, pp. 1228–1234, Mar. 2017.

[7] "IEEE P802.3ca 50G-EPON Task Force," 2016. [Online]. available. http://www.ieee802.org/3/ca/

[8] ITU-T Recommendation G.987 10-Gigabit-Capable Passive Optical Network (XG-PON) Systems, Int. Telecommun. Union, Geneva, Switzerland, 2012. [Online]. Available: https://www.itu.int/rec/T-REC-G.987.3/en, Accessed on: Oct. 16, 2017.

[9] M. S. Erkılınc, D. Lavery, B. C. Thomsen, R. I. Killey, S. J. Savory, and P. Bayvel, "Bidirectional wavelength division multiplexed transmission over installed fibre using a simplified optical coherent access transceiver," *Nature Commun.*, vol. 8, no. 1043, pp. 1–10, Oct. 2017.

[10] Y. X. Zhu *et al.*, "224 Gb/s Optical carrier-assisted Nyquist 16-QAM half-cycle single-sideband direct detection transmission over 160 km SSMF," *J. Lightw. Technol.*, vol. 35, no. 9, pp. 1557–1565, May. 2017.

[11] M. S. Erkilinc *et al.*, "Spectrally efficient WDM nyquist pulse-shaped 16-QAM subcarrier modulation transmission with direct detection," *J. Lightw. Technol.*, vol. 33, no. 15, pp. 3147–3155, Aug. 2015.

[12] Z. Li *et al.*, "Spectrally-efficient 168 Gb/s/λWDM 64-QAM single-sideband Nyquist-subcarrier modulation with Kramers-Kronig direct-detection receivers," *J. Lightw. Technol.*, vol. 36, pp. 6, pp. 1340–1346, Mar. 2018.

[13] K. Zou, Y. Zhu, F. Zhang, and Z. Chen, "Spectrally efficient terabit optical transmission with Nyquist 64-QAM half-cycle subcarrier modulation and direct detection," *Opt. Lett.*, vol. 41, no. 12, pp. 2767–70, Jun. 2016.

[14] Z. Li *et al.*, "112 Gb/s/λ WDM direct-detection Nyquist-SCM transmission at 315 (b/s)/Hz over 240 km SSMF enabled by novel beating interference compensation," in *Proc. Opt. Fiber Commun. Conf. Exhib. (OFC)*, Los Angeles, CA, USA, Mar. 2017, Paper Tu3I4.

[15] J. L. Wei, C. Sanchez, and E. Giacoumidis, "Fair comparison of complexity between a multi-band CAP and DMT for data center interconnects," *Opt. Lett.*, vol. 42, no. 19, pp. 3860–3863, Oct. 2017.

[16] J. Zhang, J. Yu, F. Li, N. Chi, Z. Dong, and X. Li, "11 × 5 × 9.3Gb/s WDM-CAP-PON based on optical single-side band multi-level multi-band carrier-less amplitude and phase modulation with direct detection," *Opt. Express*, vol. 21, no. 16, pp. 18842–18848, Aug. 2013.

[17] M. Xu *et al.*, "Orthogonal multiband CAP modulation based on Offset-QAM and advanced filter design in spectral efficient MMW RoF systems," *J. Lightw. Technol.*, vol. 35, no. 4, pp. 997–1005, Feb. 2016.

[18] J. Shi, J. Zhang, N. Chi, and J. Yu, "Comparison of 100G PAM-8, CAP-64 and DFT-S OFDM with a bandwidth-limited direct-detection receiver," *Opt. Express*, vol. 25, no. 26, Dec. 2017, Art. no. 32254.

[19] C. H. Lin *et al.*, "Simplified 27.15 Gbits/s spread-OFDM PON using DFT/IDFT-free receiver with 1/16 sub-Nyquist sampling rate," in *Proc. Opt. Fiber Commun. Conf. Exhib.*, Los Angeles, CA, USA, Mar. 2017, Paper W1K.2.

[20] C. Chen *et al.*, "Tunable optical frequency comb enabled scalable and cost-effective multiuser orthogonal frequency-division multiple access passive optical network with source-free optical network units," *Opt. Lett.*, vol. 37, no. 19, pp. 3954–3956, Oct. 2012.
[21] J. Zhang *et al.*, "Full-duplex quasi-gapless carrier aggregation using FBMC in centralized radio-over-fiber heterogeneous networks," *J. Lightw. Technol.*, vol. 35, no. 4, pp. 989–996, Feb. 2017.
[22] Z. Feng *et al.*, "Ultra-high capacity WDM-SDM optical access network with self-homodyne detection downstream and 32QAM-FBMC upstream," *Opt. Express*, vol. 25, no. 6, Mar. 2017, Art. no. 5951.
[23] A. Saljoghei, F. Gutierrez, P. Perry, D. Venkitesh, R. Koipillai, and L. Barry, "Experimental comparison of FBMC and OFDM for multiple access uplink PON," *J. Lightw. Technol.*, vol. 35, no. 29, pp. 1595–1604, May 2017.
[24] Z.-K. Weng, Y.-C. Chi, H.-Y. Wang, C.-T. Tsai, and G.-R. Lin, "75-km long reach dispersion managed OFDM-PON at 60 Gbit/s with quasi-color-free LD," *J. Lightwave. Technol.*, vol. 36, no. 12, pp. 2394–2408, Jun. 2018.
[25] S. Jung, S. Jung, and S. Han, "AMO-FBMC for reduction of multiple access interference between asynchronous ONUs in PON," in *Proc. Opt. Fiber Commun. Conf. Exhib. (OFC)*, Los Angeles, CA, USA, Mar. 2015, Paper Th2A.53.
[26] F. Mangone *et al.*, "A PAPR reduction technique using Hadamard transform combined with clipping and filtering based on DCT/IDCT for IM/DD optical OFDM systems," *Opt. Fiber Technol.*, vol. 20, no. 4, pp. 384–390, Aug. 2014.
[27] Y. Shao, N. Chi, J. Fan, and W. Fang, "Generation of 16-QAM-OFDM signals using selected mapping method and its application in optical millimeter-wave access system," *IEEE Photon. Technol. Lett.*, vol. 24, no. 15, pp. 1301–1303, Aug. 2012.
[28] Y. Xiao, M. Chen, F. Li, J. Tang, Y. Liu, and L. Chen, "PAPR reduction based on chaos combined with SLM technique in optical OFDM IM/DD system," *Opt. Fiber Technol.*, vol. 21, pp. 81–86, Jan. 2015.
[29] P. Cheng, Y. Xiao, L. Dan, and S. Li, "Improved SLM for PAPR reduction in OFDM system," in *Proc. IEEE Int. Symp. Personal Indoor Mobile Radio Commun.*, 2017, pp. 1–5.
[30] F. Li, J. Yu, Z. Cao, J. Xiao, H. Chen, and L. Chen, "Reducing the peak-to-average power ratio with companding transform coding in 60 GHz OFDM-ROF systems," *J. Opt. Commun. Netw.*, vol. 4, no. 3, pp. 202–209, Mar. 2012.
[31] A. Sahin *et al.*, "Flexible DFT-S-OFDM: Solutions and challenges," *IEEE Commun. Mag.*, vol. 54, no. 11, pp. 106–112, Nov. 2016.
[32] K. Choi, "Alamouti coding for DFT spreading-based low PAPR FBMC," *IEEE Trans. Wireless Commun.*, vol. 18, no. 2, pp. 926–941, Feb. 2019.
[33] G. Berardinelli *et al.*, "Zero-tail DFT-spread-OFDM signals," in *Proc. IEEE Globecom Workshops (GC Wkshps)*, Dec. 2013, pp. 229–234.
[34] C. Zhu, B. Corcoran, and J. L. Arthur, "Experimental comparison between Nyquist-WDM and continuous DFT-S-OFDM systems," in *Proc. Opt. Fiber Commun. Conf. Exhib.*, 2014, pp. 1–3.
[35] R. Nissel and M. Rupp, "Pruned DFT-spread FBMC: Low PAPR low latency high spectral efficiency," *IEEE Trans. Commun.*, vol. 66, no. 10, pp. 4811–4825, Oct. 2018.
[36] D. Na, and K. Choi, "DFT spreading-based low PAPR FBMC with embedded side information," *IEEE Trans. Commun.*, vol. 68, no. 3, pp. 1731–1745, Mar. 2010.
[37] Z. Liu, P. Xiao, and S. Hu, "Low-PAPR Preamble Design for FBMC Systems," *IEEE Trans. Veh. Technol.*, vol. 68, no. 8, pp. 7869–7876, Aug. 2019.
[38] A. Sahin, I. Guvenc, and H. Arslan, "A survey on multicarrier communications: Prototype filters, lattice structures, and implementation aspects," *IEEE Commun. Surveys Tut.*, vol. 16, no. 3, pp. 1312–1338, Jul.-Sep. 2014.
[39] M. Zhu *et al.*, "Optical single side-band Nyquist PAM-4 transmission using dual-drive MZM modulation and direct detection," *Opt. Express*, vol. 26, no. 6, pp. 6629–6638, Mar. 2018.
[40] T. Ihalainen, A. Viholainen, T. H. Stitz, M. Renfors, and M. Bellanger, "Filter bank based multi-mode multiple access scheme for wireless uplink," in *Proc. IEEE Eur. Signal Process. Conf. (EUSIPCO)*, Aug. 2009, pp. 1354–1358.
[41] H.-Y. Chen, C.-C. Wei, I. C. Lu, H.-H. Chu, Y.-C. Chen, and J. Chen, "High-capacity and high-loss-budget OFDM long-reach PON without an optical amplifier [Invited]," *J. Opt. Commun. Netw.*, vol. 7, no. 1, pp. A59–A65, Jan. 2014.